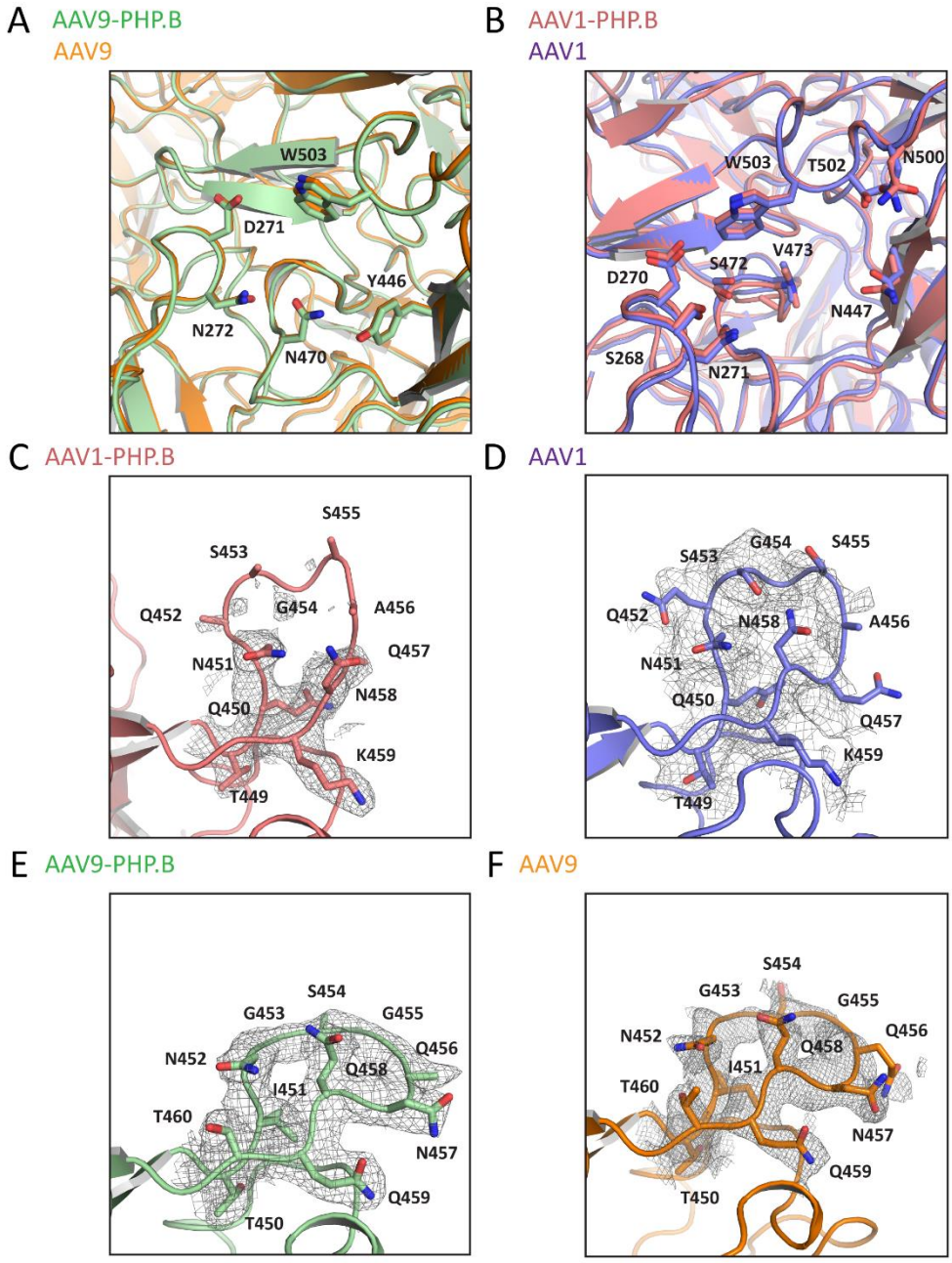

Supplemental Figure 1. Insertion of the PHP.B peptide does not alter glycan binding structures in the AAV capsid backbone but may induce changes in the adjacent HVRIV. (A) Overlay of AAV9-PHP.B (green) and AAV9 (orange) structures at AAV9's galactose-binding site. (B) Overlay of AAV1-PHP.B (salmon) and AAV1 (purple) structures at AAV1's sialic acid-binding site. Residues that play a role in glycan binding at either binding site are indicated for comparison. Electron-density map contoured at 1σ (gray mesh) and fitted model residues with identities indicated for HVR-IV of the (C) AAV1-PHP.B, (D) AAV1, (E) AAV9-PHP.B, and (F) AAV9 capsids. Electron density maps in (C-E), were obtained from cryo-EM reconstructions, and in (F) from the 2Fo-Fc X-Ray electron density map. All figures were generated using PyMol.

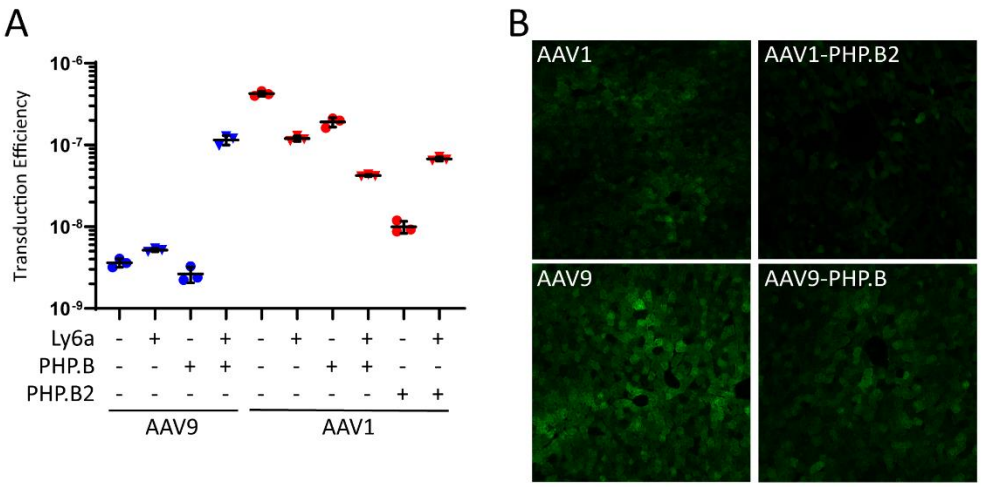

Supplemental Figure 2. Performance of AAV9-PHP.B and AAV1-PHP.B Vectors in Cell Lines and Ly6a(-) Tissues. (A) Transduction efficiency of AAV9-PHP.B and AAV1-PHP.B variants shown without normalization to cell type or wild-type capsid. This format highlights the inherent differences in transduction efficiency between AAV9 and AAV1-based capsids in HEK-293 cells. Horizontal bars represent group averages; SDs are reported as error bars; n=3. (B) AAV1-PHP.B2 and control vectors packaging a CB7-eGFP reporter gene were administered intravenously to C57BL/6J mice at a dose of 3×10^{11} GC per mouse. All vectors show widespread transduction of Ly6a(-) murine hepatocytes.